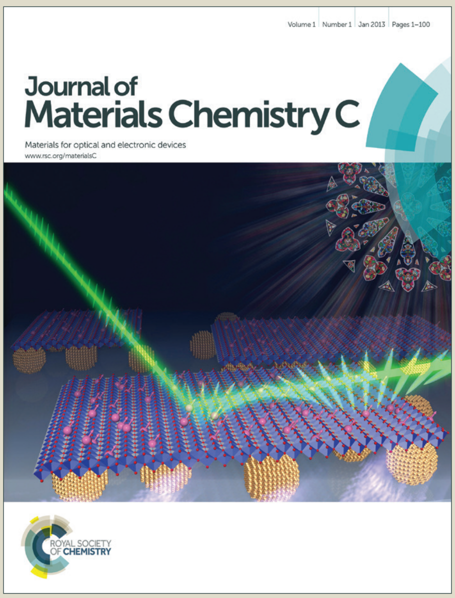

Volume 1 | Number 1 | Jan 2013 | Pages 1–100
Journal of Materials Chemistry C
Materials for optical and electronic devices
www.rsc.org/materialsC
ROYAL SOCIETY OF CHEMISTRY

Microemulsion-based synthesis of $V_{1-x}W_xO_2$@SiO_2 core-shell structures for smart window applications

Yijie Zhou[1], *Shidong Ji*[1], *Yamei Li*[1], *Yanfeng Gao*[1,2*], *Hongjie Luo*[1,2], *Ping Jin*[1*]

1 State Key Laboratory of High Performance Ceramics and Superfine Microstructure, Shanghai institute of Ceramics, Chinese Academy of Sciences, Dingxi 1295, Changning, Shanghai, 200050, China

2 School of Materials Science and Engineering, Shanghai University, Shangda Rd. 99, Baoshan, Shanghai 200444, China

* Author for correspondence. Email: yfgao@shu.edu.cn, Tel/Fax: +86-21-5241-5270;
Email: p-jin@mail.sic.ac.cn, Tel/Fax: +86-21-6990-6213

Abstract

Microemulsion technology was introduced to prepare $V_{1-x}W_xO_2$@SiO_2 core-shell nanostructures with various morphologies (nanorod, nano-sphere, and their mixture) by controlling the pH of the microemulsion. Flexible foils coated with the core-shell nanoparticles exhibited high optical performance with solar regulation efficiencies up to 12.55, 14.17, and 12.90% and fairly high visible transmittance of 53.20, 45.26 and 39.41 for 0at%, 1at%, and 2at% of W-doped VO_2 particles, respectively. The results suggested that the current foil was very suitable for application in smart windows. Interestingly, W doping did not deteriorate the solar regulation ability, which has not been reported before. The SiO_2 shell played multifunctional roles because it can not only depress the aggregation and secondary growth of the nanoparticles during the process of annealing but also obviously enhance the thermal stability of $V_{1-x}W_xO_2$. The amazing results make significant progress in VO_2-based thermochromic coating with a Mott phase transition temperature near room temperature and pave the way for practical application to smart window.

Table of Content

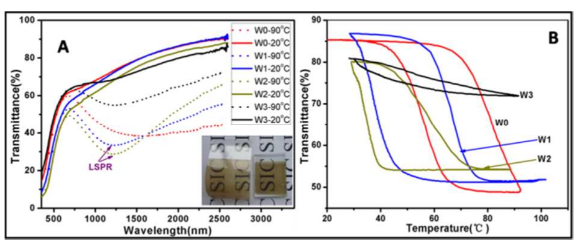

Localized surface plasmon resonance in $V_{1-x}W_xO_2$ nanoparticles can induce the excellent solar regulation efficiency of thermochromic smart windows.

Introduction

Metal oxide nanocrystals have aroused extensive attention for their outstanding optical, electrical, magnetic, and / or chemical properties that cannot be achieved by their bulk counterparts.[1-7] Among plenty of metal oxide nanocrystals, vanadium oxides are special not only for their rich structural diversity including VO_2(M1), VO_2(M2), VO_2(R), VO_2(A), VO_2(B), V_2O_3, and V_2O_5, but also for their huge potential applications in the fields of high-energy density lithium-ion batteries, catalysts, sensors, and so on.[8] The most intriguing binary compound among the numerous vanadium oxides is VO_2(M1), which exhibits a well-defined reversible metal-semiconductor phase transition near room temperature (~68°C).[9,10] The phase transition in VO_2(M1) is marked by an ultrafast alteration in electrical resistance over several orders of magnitude and a sharp change in infrared (IR) transmittance, which makes this material a promising candidate for the preparation of Mott field-effect transistors, switching devices, optical limiting elements, and smart windows.[11-15]

For practical application to smart window, several issues related to VO_2(M1) deserve consideration: its slightly high phase transition temperature (*Tc*), low visible transmittance (T_{vis}), and weak optical regulation in the IR region of the spectrum across the Mott phase transition.[4] Some techniques have been employed to optimize one aspect while sacrificing others; for example, introducing a high valence ion (W^{6+}) can obviously lower the phase transition temperature but distinctly weaken the IR regulating ability,[16] increasing the thickness of the thin film can enhance its IR regulating ability but noticeably reduce its visible transmittance.[4] It is worth mentioning that a few reports indicate that scaling the VO_2 dimension to the nanoscale can effectively lower the phase transition temperature, improve visible transmittance and maintain a relatively strong IR regulation ability.[2,3,17]

A number of chemical and physical strategies have been employed to prepare VO_2 thin films and nanoparticles in recent years. Compared to physical methods, such as sputtering[18] and ion implantation,[19] which require high input costs and exhibit low efficiencies in the preparation of qualified VO_2 thin films, chemical methods have the advantages of low cost, convenient operation, high yield, and the ability to produce on a large scale. In fact, there have been reports on chemical production methods of VO_2 thin films and nanoparticles by polymer assisted deposition (PAD),[4,20,21] direct thermolysis of VO_2 precursors,[22,23] and hydrothermal synthesis.[2,3] The use of PAD has obtained nanoporous high-qualified VO_2 thin films with excellent optical properties but failed to produce films with a large area. The direct thermolysis of VO_2 precursors cannot obtain well-dispersed VO_2(M1) nanoparticles. Hydrothermal synthesis has been well developed for VO_2(M1) nanoparticles synthesis, and these nanoparticles have been successfully applied to make polymer-based flexible VO_2(M1) thermochromic films.[3,24,25] However, the disadvantages of the hydrothermal method are obvious. Apart from the time-consuming reaction process for well-crystallized VO_2(M1) and complex large scale post-treatments, an additional surface treatment step is required to enhance the chemical stability of VO_2(M1) nanoparticles because they are metastable and easily oxidized into V_2O_5 in wet air after long time periods. Furthermore, an inevitable problem is that owing a high *Tc* is unacceptable for the practical application of VO_2-based foils, and decreasing *Tc* to near room temperature with doping cannot maintain sufficiently high solar regulation efficiencies.

In this study, a microemulsion-based method was developed to prepare VO_2 nanostructures for the first time. Compared with hydrothermal methods, microemulsion method is liable to operate, allow for easy control over size and morphology, and can be completed quickly; meanwhile, VO_2 nanoparticles can be directly coated by SiO_2 in a single solution. SiO_2, as a transparent protective shell, plays multifunctional roles because it can not only prevent from agglomeration and secondary growth in the process of thermal treatment but also enhance the chemical stability of VO_2(M1) and improve visible transmittance. An amazing novelty of our study was that films prepared by $V_{1-x}W_xO_2$@SiO_2 with a low value of x (such as x=1% or 2%) show a decreased Mott phase transition temperature and improved solar regulation performance, which was not yet reported before. In brief, the microemulsion-based method is a great breakthrough for the production of VO_2-based foils and provides a new way for optimizing smart windows.

Experiments and Methods

Preparation of $VOCl_2$ solution

The $VOCl_2$ solution was prepared by the reduction of commercial vanadium pentoxide (V_2O_5, 99%, Sinopharm Chemical Reagent) with hydrazine monohydrate ($N_2H_4 \cdot H_2O$, 99%, Sigma) in the presence of hydrochloric acid (HCl, AP, Sinopharm Chemical Reagent). Typically, 100.0 mL of 1 M HCl solution and 10.0 g of V_2O_5 were mixed under magnetic stirring at 60 °C; 2.0 mL of hydrazine monohydrate was slowly dropped into the above mixed solution. The reaction was kept for 2 h until the solution was transparent blue, indicating that V^{5+} had been reduced to V^{4+}. The final solution was collected in a 100 mL volumetric flask.

Preparation of VO_2@SiO_2 nanostructures

For the synthesis of VO_2@SiO_2 nanostructures, reverse microemulsions were prepared by mixing 100.0 mL of N-decane (97%, Aladdin) as a non-polar phase, 4.0 g of cetyltrimethylammoniumbromide (CTAB, 99%, Aladdin) as a surfactant, 10.0 mL of 1-hexanol (98%, Aladdin) as a cosurfactant, and 5.0 mL of V^{4+} solution prepared as described above as the polar phase. The compositions of our microemulsion were mainly taken from work by Feldman.[5] The microemulsion system was heated to 60 °C in air. After 30 min of magnetic stirring, a certain amount of 1 M ammonia ($NH_3 \cdot H_2O$, Sinopharm Chemical Reagent) was slowly dropped to exactly control the pH of the microemulsion, and the temperature was increased to 100 °C within 10 min and maintained for 1-2 h. When the solution was cooled to near room temperature, 0.5 ml of tetraethyl orthosilicate (TEOS, AR, Aladdin) was added to the above solution and stirred for another 2-4 h. Finally, 40 ml of diethylene glycol (DEG, CP, Sinopharm Chemical Reagent) was added in order to depress the reaction and to initiate a phase separation. The composites were collected from the DEG bottom phase by centrifugation. The solid was washed several times by redispersion in ethanol and centrifugation and finally dried in an oven at 110 °C for 2 h. The reaction conditions and resulting morphologies of precursors were listed in Table 1. To obtain well-crystallized VO_2 powders, annealing was required to elevate from room temperature to 600-800 °C for 200-300 seconds by program control, and then maintained at 600 and 800 °C for 1-3 h in N_2 atmosphere.

Preparation of $V_{1-x}W_xO_2$@SiO_2 nanostructure

Solutions with different molar ratios of W^{6+} to V^{4+} were prepared by mixing ammonium paratungstate ($(NH_4)_{10}H_2(W_2O_7)_6 \cdot H_2O$, AP, Aladdin) with $VOCl_2$ solution. The subsequent steps were the same as those for the preparation of the VO_2@SiO_2 nanostructures. Samples W0, W1, W2, and W3 indicate that the addition molar ratio of W:V is 0, 1, 2, and 3%, respectively. The addition amount and the corresponding molar ratio of W^{6+} in final products were listed in Table 2.

Characterization

The crystal phases of the final products were identified using a Rigaku Ultima IV X-ray diffractometer (XRD) with Cu Kα radiation (λ=1.5418 Å). The morphology was characterized by transmission electron microscopy (TEM, JEM 4000EX, JEOL, Tokyo, Japan). The W doping concentrations were detected by inductively coupled plasma (ICP, Thermoelectric Corporation, IRIS Intrepid). The phase transition properties of the resulting products were measured by differential scanning calorimetry (DSC200F3, NETZSCH) with the temperature ranging from 0 to 100 °C at a heating/cooling rate of 10 $^{o}C \cdot min^{-1}$, using a liquid nitrogen cooling unit. The thermochromic properties were evaluated by coating the powder onto a float glass substrate. For measurements, the powders were coated on a slide of glass uniformly by a double-sided adhesive and highly transparent Teflon tape, which exhibits no thermochromic property. The transmittance curve of a glass slide solely coated with a piece of tape was calibrated as a baseline. The transmission measurements were conducted at wavelengths ranging from 250 to 2600 nm at 25 and 100 °C on a UV-Vis spectrophotometer (HITACHI U-3010) by inserting the films in a temperature controlling unit.

For all the samples, the integrated luminance transmittance (T_{lum}, 400-700 nm), and solar transmittance (T_{sol}, 240-2600 nm) were obtained based on the measured spectra using the following equation:

$$T_{\rho} = \int \psi_{\rho}(\lambda)T(\lambda)d\lambda \,/ \int \psi_{\rho}(\lambda)d\lambda$$

where T(λ) is the transmittance at wavelength λ; ρ denotes *lum* or *sol* for the calculations; Ψ_{lum} is the standard efficiency function for photopic vision; and Ψ_{sol} is the solar irradiance spectrum for an air mass of 1.5 (corresponding to the sun standing 37° above the horizon).

Results and discussion

During the process of adding diluted ammonia, the colour of the microemulsion transformed from blue to pink, to brown and finally to black with a gradual increase of pH, as displayed in Figure 1. The different colours of the solution reflected various polymerization and coordination relationships between V^{4+} and other anions, which are common in vanadium aqua complexes.[26] Figure 2 showed TEM images of VO_2@SiO_2 nanostructures obtained at different pH values. When the microemulsion was acidic (pH≈6), the shape of VO_2 precursor was only nanorod with a small width less than 20 nm and a length of about 200 nm; when the solution was alkaline (pH≈10), nearly spherical particles were formed, with an average diameter less than 20 nm. At pH≈8, the final product was a mixture of nanorods and nano-spherical particles. Keeping other conditions constant and only adjusting the pH of the microemulsion, VO_2 precursors with different morphologies were obtained, which indicated that pH played a vital role in determining the shape of VO_2 precursor.

In microemulsion systems, it is common to obtain nano-spherical particles because microemulsion micelles are generally spherical liquids and prone to yield spherical particles.[5] Under our experimental conditions, V^{4+} can exist in the form of $V_xO_y^{z-}$ in an alkaline environment, which easily constructs a cage structure and finally forms a spherical precursor.[26,27]

To make nanorod evolution clear under acidic conditions, a contrasting experiment was carried out. When adding ammonia into the microemulsion solution until the pH was close to 6, diethylene glycol (DEG) was quickly introduced to the solution to depress the morphology change of the nanostructures.[5] Subsequently, the VO_2 precursor was dispersed into alcohol and coated with SiO_2. The morphology of the VO_2 precursor still maintained the nanorod shape (Figure 2D). The short-term experiment elucidated that the nanostructure was internally directed by the pH of the solution.

As for the morphology evolution of a crystal whose morphology is dependent on the initial seed during the nucleation process and its surface energy for the growth of nanocrystals, many factors can play critical roles, such as pH,[28] the identity of the surfactant,[29] temperature[30] and a combination of the above.[31] Conversely, the growth of amorphous nanostructures is often correlated with the condensation of monomers owing to the attraction of positively and negatively charged groups. For our experiment, when the pH was elevated from 1 to 6, the solution gradually transformed from transparent blue to turbid pink, which indicated the emergence of the solid VO_2 precursor. As the pH was increased further, the colour of the microemulsion became black. The colour transformation indicated the different condensation styles of V^{4+}.[32,33] It was reported that V^{4+} existed in the form VO^{2+} in strongly acidic solutions. As the pH increased, VO^{2+} attracted hydroxyl groups and water molecules and finally became solid VO_2 through condensation reactions.[34]

The formation mechanism of VO_2 precursor nanorod can be explained by considering six-coordinated zero-charge monomers $[VO(OH)_2(OH_2)_3]$ in equilibrium with the decavanadate. That the $[VO(OH)_2(OH_2)_3]$ is chosen as the reactive monomer is mainly because its simplicity and validity. The positive VO^{2+} can combine with two negative hydroxyl groups (－OH) to keep neutral due to Couloub attraction; vanadium ion is six-coordinated and needs to attract another three non-charged water molecules to keep stability. As soon as the monomers－$[VO(OH)_2(OH_2)_3]$ appear in solution, these entities could be condensed by olation and oxolation; olation reactions, in which labile water molecules are apt to break away, are kinetically faster than oxolation reactions.[34] The formation of chains is the result of the structure of the precursors; short V=O bonds prevent condensation along their axis since V=O bonds destroy the nucleophilic character of such ligands, leaving them only slightly basic and not prone to protonation. The zero-charge monomers $[VO(OH)_2(OH_2)_3]$ can be condensed along the directions of V-OH and V-OH_2, where V-OH_2 is more liable for condensation.[34-36] The styles of condensation could be summarized in Scheme 1, and

Scheme 2 gave a possible formation mechanism of VO_2 nanorod from $[VO(OH)_2(OH_2)_3]$.

For practical applications in smart windows, decreasing *Tc* to near room temperature (RT) is necessary, and W^{6+}, as the most effective doping ion, was chosen to partially replace V^{4+} ions in our experiment. To investigate the crystallization of nanoparticles, Figure 3A shows powder XRD patterns of $V_{1-x}W_xO_2@SiO_2$. The XRD patterns could be indexed to monoclinic VO_2(M1) (JCPDS No. 043-1051). The (001) peak was thoroughly covered with its leftmost peak (-111), which first emerged through the thermal treatment process,[23,24] indicating that the obtained VO_2(M1) was small in size, which can also easily be obtained with hydrothermal methods.[2,3,24,25] Figure 3B illustrated the XRD patterns of $V_{1-x}W_xO_2@SiO_2$ with a relatively slow scanning speed (0.1 degree per minute) in the range of 26.5° to 29.5°. With increasing W-doped content, the (011) peak was blue-shifted, suggesting that the interplanar distance of (011) increased. Note that the radius of W^{6+} is larger than that of V^{4+}. This finding clearly shows that the W atoms successfully substitute for V atoms in the VO_2 lattice.

Figure 4(A, B) showed the morphology changes of $VO_2@SiO_2$ precursor after thermal treatment. During the crystallization process, the amorphous VO_2 precursor had diverse transformations. Some nanorods burst into extremely small nanoparticles (< 3 nm) that were embedded in SiO_2; some shrunk owing to a difference in density between the amorphous precursor and crystalline VO_2(M1), which led to the formation of some void spaces (Figure 4B) between the VO_2 core and SiO_2 shell. Figure 4(C, D) showed a lattice-resolved HRTEM image and SAED pattern of an individual VO_2(M1) nanorod after heat treatment. Both characterizations corroborated the single crystalline nature of the nanostructures.

Figure 5(A, B) showed TEM images of W-doped $VO_2(M1)@SiO_2$, which suggested that VO_2(M1) nanorods were completely coated by SiO_2 (see the insets in Figure 5(A, B)). The inset of Figure 5B presented that amorphous VO_2 nanorods changed into a small string of VO_2(M1) beads after the crystallization process. It can be seen from Figures 4(A, B) and 5(A, B) that the VO_2 precursors were gradually shaped into VO_2(M1) nano-spherical particles with increasing W-doped content. The morphology evolution with the variation of pH after heat treatment were summarized in Scheme 3.

Metallic oxide shells such as TiO_2, SiO_2 provide several inherent advantages when combined with VO_2 nanoparticles, such as high stability, optical transparency, and easy regulation of the coating process.[3] However, TiO_2 is not suitable to coat on the surface of VO_2(M1) in practical applications because the photocatalytic activity of TiO_2 makes it possible to slowly decompose transparent organic resin under solar radiation. Therefore, inert SiO_2 is selected as a protection shell.

In this study, SiO_2 shell is aimed at preventing VO_2 precursor from agglomeration during the annealing because SiO_2 owes a high melting point (> 1700 ^{o}C) at an atmospheric pressure, and meanwhile can enhance the chemical stability of VO_2(M1) nanoparticles for practical application. Another advantage of SiO_2 is owing to its wide band gap (> 8 eV), which allows the transmitting of visible and IR light, similar with the effect of introducing nanoporosity in VO_2(M1) thin films.[21] To illustrate that SiO_2 can enhance thermal stability of thermochromic nanopaticles, uncoated VO_2(M1) and $V_{1-x}W_xO_2$@SiO_2 annealed at 300 °C for 2 h in air were conducted. XRD patterns in Figure 6 confirmed that the uncoated VO_2(M1) was completely oxidized and SiO_2-coated $V_{1-x}W_xO_2$ had avoided oxidation, which demonstrated that the SiO_2 shell can serve as a barrier layer for oxygen diffusion.

Most papers in the literature have focused on the reduction value 20-23°C/at %W for a single crystal, and our results were in accordance with these reports (Table 3).[2,16] The mechanism of decreasing the *Tc* by W doping has been well explained by Tan's study[37] which suggested that replacing V atom with W atom in VO_2 crystal lattice can induce high symmetry around W atom, implying the transformation to a rutile-like structure. The symmetric W core drives the detwisting of the nearby asymmetric monoclinic VO_2 lattice to form rutile-like VO_2 nuclei, and the propagations of these W-encampassed nuclei through the matrix lower the thermal energy barrier for phase transition. One interesting phenomenon arousing our attention in this study was that without W^{6+} doping, *Tc* of VO_2 *was* raised when VO_2 was transformed from the semiconductor to metal direction (on heating) from the normal value of 68 °C to as high as 81.3 °C. This result was similar to that reported in the literature.[19] Vanadium dioxide nanocrystals showed a rise in *Tc* when they were implanted into a fused silica matrix. The compressive stress between SiO_2 and VO_2 can induce the rise of *Tc*,[38,39] which is the main factor for the rise of *Tc*.

To demonstrate our hypothesis, simple experiments were carried out. Extending the thermal treatment time can lower the phase temperature to about 68 °C. Moreover, the value of *Tc* decreased by several degrees after continuous DSC cycling measurements for 20 times owing to the relaxation of the strain. It is not easy to calculate the concrete compressive strain of a single VO_2(M1)@SiO_2 composite particle. For simplifying calculation, we can estimate the average strain according to the variation of phase transition temperature (the measuring temperature minus the theoretical temperature), which has been studied in detail by other groups.[40,41] Taking VO_2(M1)@SiO_2 as an example, the average strain of a composite particle approximately equals to (81.3-67)/12 GPa=1.19 GPa.[40]

To investigate the optical properties of $V_{1-x}W_xO_2$@SiO_2 nanoparticles, sandwich films were prepared by coating composite powders onto highly transparent Teflon tape. Figure 8A showed the optical spectra of $V_{1-x}W_xO_2$@SiO_2 films. Figure 8B showed the thermal hysteresis at 2000 nm. Keeping the visible spectrum transmittance above 40%, the solar modulation efficiency (ΔT_{Sol} %) was 12.55%. This value is closer to ideal, considering that it is much higher than 4.4% for a single-layered VO_2 film, 7.0% for a TiO_2/VO_2 double-layered film[42] and 12.1% for a $TiO_2/VO_2/TiO_2/VO_2/TiO_2$ five-layered film[43] prepared by the sputtering method or 7.4% for a typical single-layered VO_2 film prepared by a solution-based method.[44] The slightly large hysteresis width appears because the heterogeneous nucleation with smaller precipitates is thermally delayed and needs larger thermal driving forces to induce the transition.[45]

A novelty in our experiment was that VO_2(M1) with a small amount of W doping did not decrease the value of ΔT_{Sol} % but rather improved it, in contrast to the results reported by our group and others.[2,46-47] This can be explained as following: free electrons at sufficient density will be confined to the surface of W-doped VO_2(R) nanoparticles at temperatures higher than *Tc*, taking participate in resonance, collective oscillations when excited by incident light known as localized surface plasmon resonance (LSPR). The final result is that the NIR is strongly absorbed, which is similar to optical absorption of noble metal nanoparticles in visible region.[49] Increasing W-doped amount can increase the density of free electrons on the surface of VO_2(R) nanoparticles, and the absorption in IR region is increasingly obvious, which can be observed in the transmittance spectra of our samples (Figure 8A, the arrows). The shape of concavity in the transmittance spectra reflects the contribution of LSPR, which agreed with reports in the literature.[49,50] Because short wavelength regions carry more energy based on the solar radiation spectrum, naturally, W-doped VO_2(M1)@SiO_2 film improves the solar regulation efficiency. However, excessive W-doped VO_2(M1) deteriorated the solar regulation efficiency (Sample W3) for serious lattice variation, which is similar with most reported results.[2,47,48,51]

Conclusions

In summary, a microemulsion-based method was introduced to prepare high performance $V_{1-x}W_xO_2$@SiO_2 composites for the first time. The morphology (nanorod, nano-sphere and their mixture) of VO_2 precursors can be easily controlled by controlling the pH of the microemulsion. The SiO_2 shell is a prerequisite because of its multifunctional roles in preventing VO_2(M1) nanoparticles from agglomeration and second growth in the crystallization process and strengthening the thermal stability of $V_{1-x}W_xO_2$ nanoparticles. A small amount of W-doped VO_2(M1) can lower the phase transition to about room temperature without weakening the solar regulation efficiency. This finding has not been reported previously. Flexible VO_2-based foils coated with $V_{1-x}W_xO_2$@SiO_2 composites have obtained excellent solar modulation efficiencies. Recently, the performance of the $V_{1-x}W_xO_2$@SiO_2-based foils was further improved. The *Tc* and solar regulation ability values of 32 ^{o}C and >12% were observed, respectively, which can be seen in Supporting Information.

Acknowledgments

This study was financially supported in part by MOST (2012AA030305, 2012BAA10B03), and the National Natural Science Foundation of China (NSFC, contract No: 51032008, 51272273, 51102270, 51272271, 51325203).

Supporting Information

Our recent optical transmittance spectra and DSC curves were shown in Supporting Information.

References

1 J. Park, S. G. Kwon, Y. J. Jang, T. W. Hyeon, Angew. Chem. Int. Ed., 2007, 46, 4630.

2 S. D. Ji , F. Zhang , P. Jin, Sol. Energy Mater. Sol. Cells, 2011, 95, 3520.

3 Y. F. Gao, S. B. Wang, H. J. Luo, L. Dai, C. X. Cao, Y. L. Liu, Z. Chen, K. Minoru, Energy Environ. Sci. , 2012, 5, 6104.

4 Z. T. Zhang, Y. F. Gao, Z. Chen, J. Du, C. X. Cao, L. T. Kang, H. J. Luo, Langmuir, 2010, 26, 10738.

5 H. Gröger, F. Gyger, P. Leidinger, C. Zurmühl, C. Feldmann, Adv. Mater, 2009, 21, 1586.

6 J. Park, N. M. Hwang, M. Kang, Y. S. Hwang, J. G. Park, J. Y. Kim, J. H. Park, Angew. Chem. Int. Ed., 2005, 44, 2872.

7 F. Gyger, M. Hubner, C. Feldmann, Chem. Mater., 2010, 22, 4821.

8 C. Z. Wu, Y. Xie, Energy Environ. Sci., 2010, 3, 1191.

9 F. J. Morin, Phys. Rev. Lett., 1959, 3, 34.

10 J. B. Goodenough, J. Solid State Chem., 1971, 3, 490.

11 S .Surnev, M. G. Ramsey, F. P. Netzer, Prog. Surf. Sci., 2003, 73, 117.

12 M. Winter, O. B. Jurgen, M. E. Spahr, P. Novak, Adv. Mater., 1998, 10, 725.

13 R. Lopez, L. A. Boatner, T. E. Haynes, L. C. Feldman, R. F. Haglund, Jr. J. Appl. Phys., 2002, 92, 4031.

14 R. Lopez, L. C. Feldman, R. F. Haglund, Jr. Phys. Rev. Lett., 2004, 93, 177403/1.

15 J. H. Kim, C. Y. Ko, A. Frenzel, S. Ramanathan, J. E. Homan, Appl. Phys. Lett.,

2010, 96, 213106.

16 M. A. Sobhan, R. T. Kivaisi, B. Stjerna, C. G. Granqvist, Sol. Energy Mater.Sol. Cells, 1996, 44, 451.

17 D. Lei, C. X. Cao, Y. F. Gao, H. J. Luo, Sol. Energy Mater. Sol. Cells, 2011, 95, 712.

18 P. Jin, S. Tanemura, Jpn. J. Appl. Phys., Part 1 1994, 33, 1478.

19 R. Lopez, L. A. Boatner, Phys. Rev. B, 2002, 65, 224113-1.

20 L. T. Kang, Y. F. Gao, H. J. Luo, ACS Appl. Mater. Interfaces, 2009, 1, 2211.

21 L. T. Kang, Y. F. Gao, Z. T. Zhang, J. Du, C. X. Cao, Z. Chen, H. J. Luo, J. Phys. Chem. C, 2010, 114, 1901.

22 C. M. Zheng, X. M. Zhang, J. H. Zhang, K. R. Liao, J. Solid State Chem., 2001, 156, 274.

23 Z. F. Peng, W. Jiang, H. Liu, J. Phys. Chem. C, 2007, 111,1119.

24 Y. F. Gao, C. X. Cao, D. Lei, H. J. Luo, K. Minoru, Y. Ding, L. W. Zhong, Energy Environ. Sci., 2012, 5, 8708.

25 Y. F. Gao, S. B. Wang, L. T. Kang, Z. Chen, J. Du, X. L. Liu, H. J. Luo, K. Minoru, Energy Environ. Sci., 2012, 5, 8234.

26 J. P. Jolivet, Metal Oxide Chemistry and Synthesis, 4rd,Masson, Paris(2000).

27 G. K. Johnson, E. O. Schlemper, J. Am. Chem. Soc., 1978, 100, 3645.

28 C. H. Lu, M. C. Wen, J. Alloys and Compounds, 2008, 448, 153.

29 M. P. Pileni, Nature Mater., 2003, 2, 145.

30 Y. Jun, Y. Jung, J. Cheon, J. Am. Chem. Soc., 2002, 124, 615.

31 S. M. Lee, S. N. Cho, J. W. Cheon, Adv. Mater., 2003, 15, 441.

32 L. Meites, J. Am. Chem. Soc., 1953, 75, 6059.

33 A. Komura, Bull. Chem. Soc. Japan, 1977, 50, 2927.

34 J. Livage, Materials, 2010, 3 , 4175.

35 P. Souchay, Thermodynamique Chinique, 3rd. Masson, Paris(1968).

36 J. J. Legendre, J. Livage, J. Colloid Interface Sci., 1983, 94, 75.

37 X. G. Tan, T. Yao, R. Long, Z. H. Sun, Y. J. Feng, H. Cheng, X. Yuan, W. Q. Zhang, Q. H. Liu, C. Z. Wu, Y. Xie, S. Q. Wei, Sci. Rep., 2012, 2, 466.

38 J. Cao, E. Ertekin, V. Srinivasan, W. Fan, S. Huang, H. Zheng, W. L. Yim, D. R. Khanal, D. F. Ogletree, J. C. Grossman, J. Wu, Nature nanotech., 2009, 4, 739.

39 W. Fan, S. Huang, J. Cao, E. Ertekin, C. Barrett, D. R. Khanal, J. C. Grossman, J. Wu, Phys. Rev. B, 2009, 80, 241105.

40 Y. Muraoka, Z. Hiroi, Appl. Phys. Lett., 2002, 80, 583

41 J. Wei, Z. H. Wang, W. Chen, David H. Cobden, Nat. Nanotech., 2009, 4, 420

42 P. Jin, G. Xu, M. Tazawa, K. Yoshimura, Jpn. J. Appl. Phys., Part 2, 2002, 41, 278.

43 N. R. Mlyuka, G. A. Niklasson, C. G. Granqvist, Sol. Energy Mater. Sol. Cells, 2009, 93, 1685.

44 Z. Chen, Y. F. Gao, L. T. Kang, J. Du, Z. T. Zhang, H. J. Luo, H. Y. Miao, G. Q. Tan, Sol. Energy Mater. Sol. Cells, 2011, 95, 2677.

45 M. M. Qazilbash, M. B., B. G. Chae, P. C. Ho, G. O. Andreev, B. J. Kim, S. J. Yun, M. B. Maple, F. Keilmann, H. T. Kim, D. N. Basov, Science, 2007, 318, 1750.

46 T. D. Manning, I. P. Parkin, M. E. Pemble, D. Sheel, D. Vernardou, Chem. Mater., 2004, 16, 744.

47 P. Jin, S. Nakao, S. Tanemura, Thin Solid Films, 1998, 324, 151.

48 P. Jin, S. Tanemura, Thin Solid Films, 1996, 281,239.

49 M. Maaza, O. Nemraoui, C. Sell, A. C. Beye, Gold Bulletin, 2005 , 38, 100.

50 G. Xu, Y. Chen, M. Tazawa, P. Jin, J. Phys. Chem. B, 2006, 110, 2051.

51 T. J. Hanlon, J. A. Coath, M. A. Richardson, Thin Solid Films, 2003, 436, 269.

Table 1 Reaction conditions and final morphologies of $VO_2@SiO_2$ precursors in microemulsion system

Sample	pH	Time（h）	Morphology
A	6	2	Nanorod
B	8	2	Nanorod, Nano-spherical particle
C	10	2	Nano-spherical particle

Table 2 The addition amount of W concentration and the corresponding molar ratio of W:V in final products

Samles	Addition amount (% atom)	Final doping ratios (% atom)
W1	1.00%	0.91%
W2	2.00%	1.63%
W3	3.00%	2.36%

Table 3 DSC peaks measured during cooling and heating for samples

Sample	Temperature (^{o}C)	
	endothermic peak	exothermic peak
W0	81.3	59.0
W1	61.7	36.2
W2	43.1	25.1
W3	34.1	23.8

Table 4 Phase transition temperature and optical properties of thermochromic foils

Sample	Tc (^oC)	T_{lum} (%)		T_{sol} (%)		ΔT_{2000nm} (%)	ΔT_{Sol} (%)
		T>Tc	T<Tc	T>Tc	T<Tc		
W0	81.3	52.24	53.12	47.13	59.68	45.70	12.55
W1	61.7	43.90	44.60	40.54	54.71	39.90	14.17
W2	43.1	39.08	39.26	36.88	49.78	31.80	12.90
W3	34.1	55.23	55.60	48.83	52.55	15.20	3.72

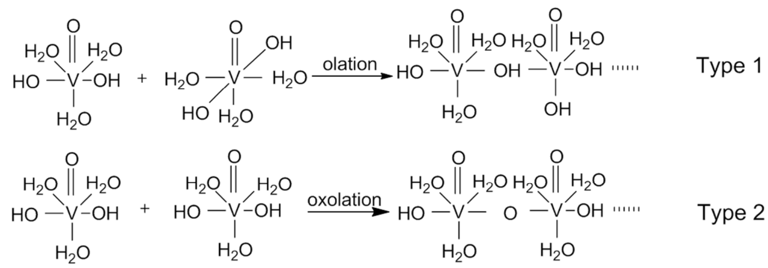

Scheme 1 the style of olation and oxolation

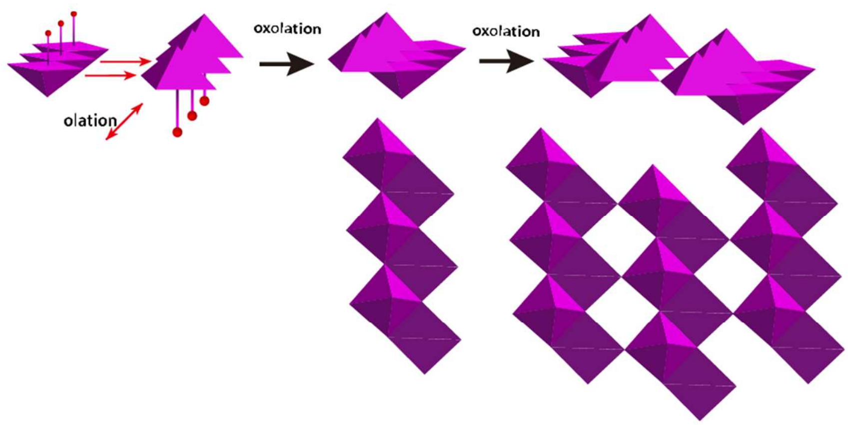

Scheme 2 Possible formation mechanism of VO_2 nanorods from $[VO(OH)_2(OH_2)_3]$

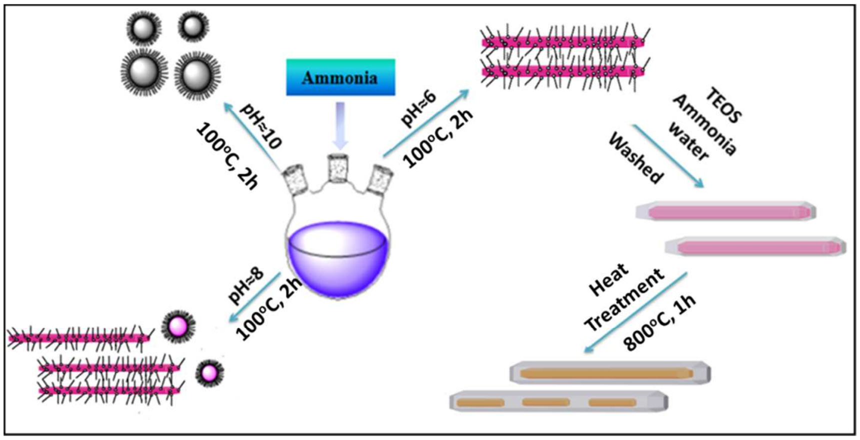

Scheme 3 The morphology evolution of $VO_2@SiO_2$ corresponding to different pH and heat-treatment condition in N_2 atmosphere

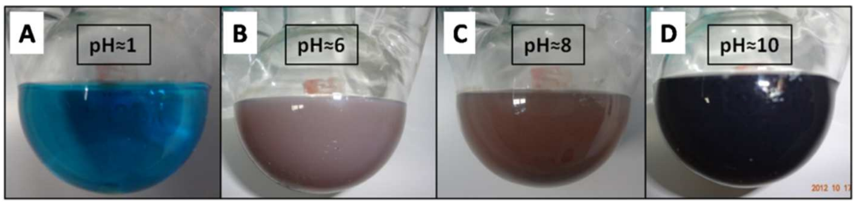

Figure 1 the microemulsion colour corresponding to different pH values; (A) without adding ammonia at pH≈1; (B, C, D) corresponding to different pH after the reaction time at 100^{o}C for 2 h.

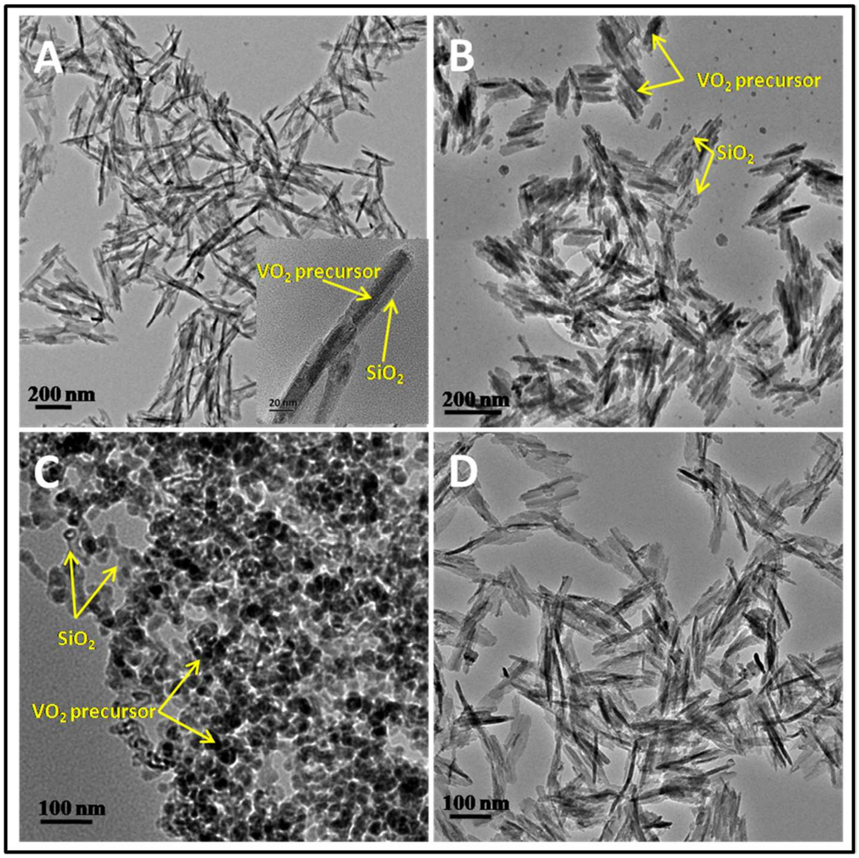

Figure 2 TEM images of VO_2@SiO_2 precursors prepared at different pH values with a reaction time of 2 h at 100^{o}C in A, B, C and a shorter time in D; (A, D) pH≈6, (B) pH≈8, (C) pH≈10; The TEM image inset in Figure 2A is a typical nanorod of VO_2@SiO_2 precursor.

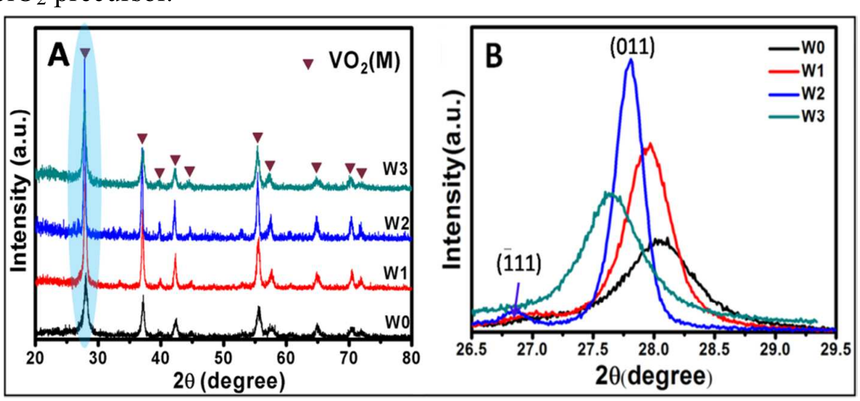

Figure 3 (A) XRD patterns of $V_{1-x}W_xO_2$@SiO_2 after heat treatment at 800°C for 1 h in N_2 atmosphere with various W-doped content; the molar ratio of W:V is 0, 1, 2, and 3% for W0, W1, W2, and W3, respectively, (B) magnified patterns (marked in 3A) of the (011) peak at a slow scanning speed of 0.10^{o} per minute from 26.5° to 29.5°.

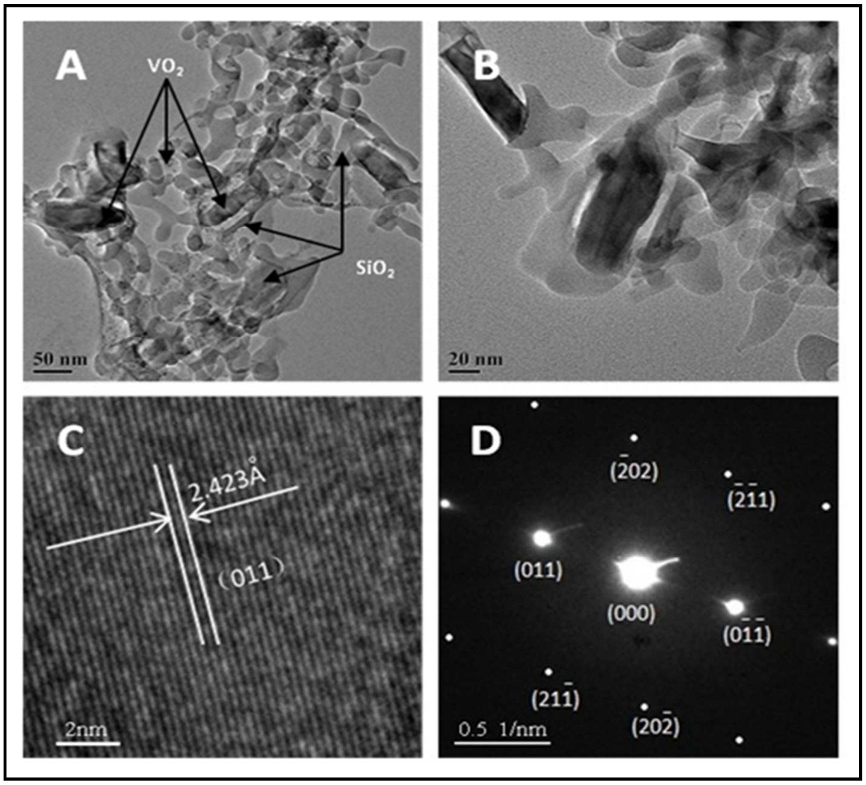

Figure 4 (A, B) TEM images of Sample W0 after heat treatment at 800°C for 1 h in N_2 atmosphere and Sample W0 meant VO_2(M1) without W doping; (C) Lattice-resolved HRTEM image of an individual VO_2(M1) nanorod showing the separation between (011) planes; (D) SAED pattern acquired for the same nanorod.

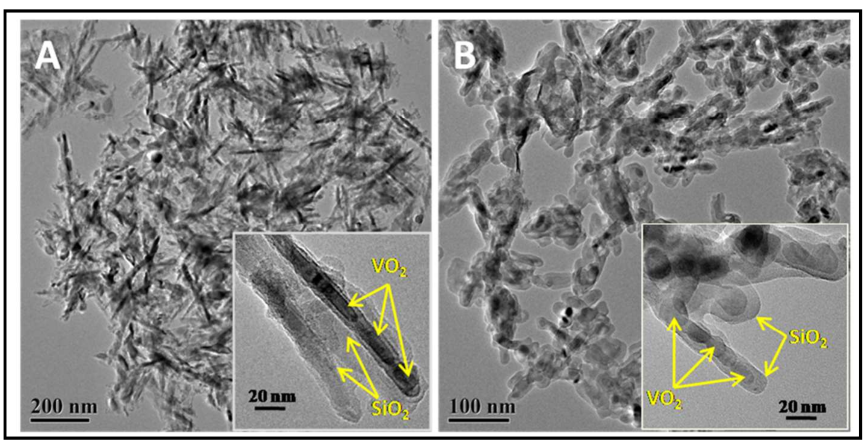

Figure 5 (A, B) TEM images of Sample W1 and W3 after thermal treantment at 800 °C in N_2 atmosphere for 1 h; W1, W3 correspond that the adding molar ratio of W:V is 1%, 3%, respectively.

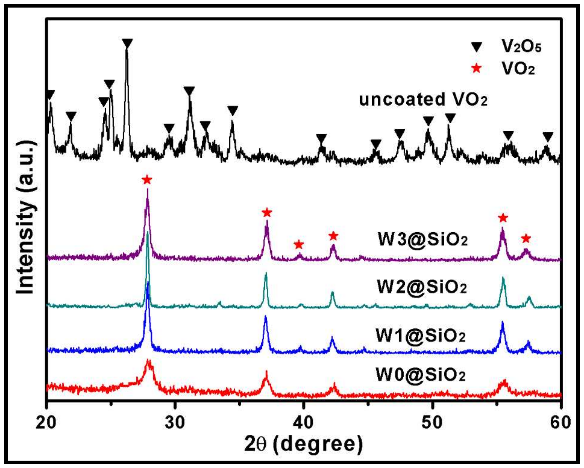

Figure 6 XRD patterns of VO_2 and $V_{1-x}W_xO_2@SiO_2$ after annealing at 300°C for 2 h in air; W0@SiO_2, W1@SiO_2, W2@SiO_2, and W3@SiO_2 mean W-doped VO_2 coated by SiO_2 with the W:V molar ratio were 0%, 1%, 2%, 3%, respectively.

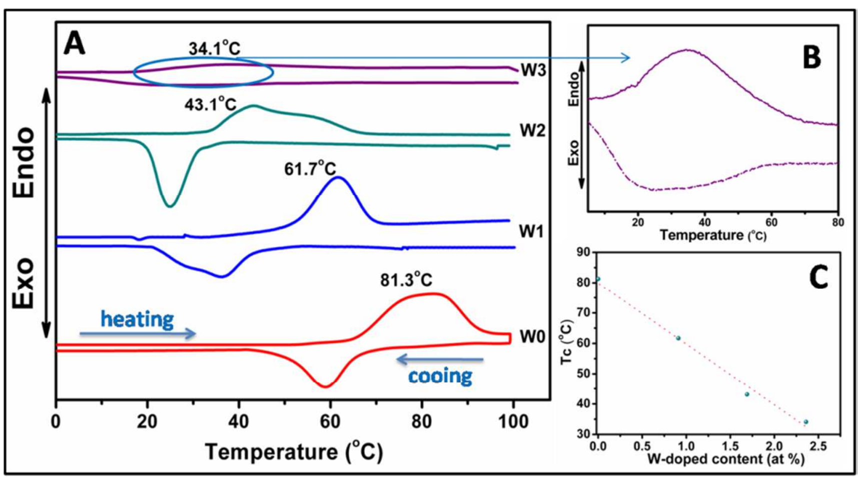

Figure 7 (A) DSC curves of $V_{1-x}W_xO_2@SiO_2$, W0, W1, W2, W3 indicate that the adding molar ratio of W:V is 0, 1, 2, and 3%, respectively; (B) A local magnified image of sample W3 (marked in 7A); (C) The plot of the phase transition temperature (*Tc*) as function of W composition x for $V_{1-x}W_xO_2$ particles.

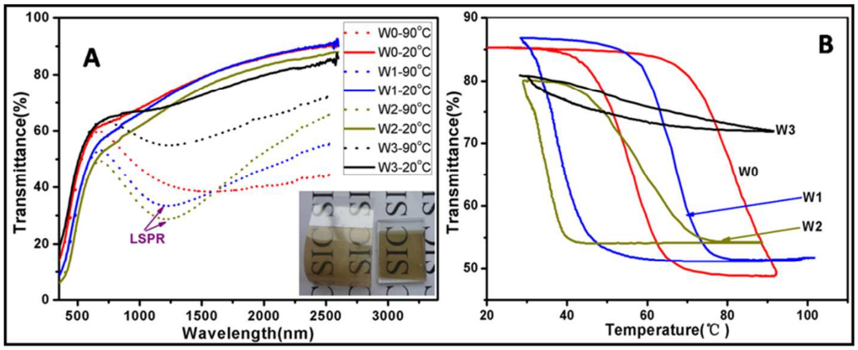

Figure 8(A, B) Optical transmittance spectra and temperature dependence of optical transmittance at a fixed wavelength (2000 nm) for $V_{1-x}W_xO_2$@SiO_2. The inserted image shows films coated by sample W2. W0, W1, W2, W3 indicate that the adding molar ratio of W:V is 0, 1, 2, and 3%, respectively.